Solution Structure of the Exocyclic 1,N^2-Propanodeoxyguanosine Adduct opposite Deoxyadenosine in a DNA Nonamer Duplex at pH 8.9. Model of pH-Dependent Conformational Transition†

Ping Huang,‡ Dinshaw J. Patel,§ and Moisés Eisenberg*,‡

Department of Pharmacological Sciences, School of Medicine, State University of New York at Stony Brook, Stony Brook, New York 11794-8651, and Department of Biochemistry and Molecular Biophysics, College of Physicians and Surgeons, Columbia University, New York, New York 10032

Received August 14, 1992; Revised Manuscript Received November 16, 1992

ABSTRACT: The solution structure of the complementary d(C1-A2-T3-G4-X5-G6-T7-A8-C9)·d(G10-T11-A12-C13-A14-C15-A16-T17-G18) DNA duplex (designated X·A 9-mer), which contains a 1,N^2-propanodeoxyguanosine exocyclic adduct X5 opposite deoxyadenosine A14 at the center, is pH dependent [Kouchakdjian, M., Eisenberg, M., Live, D., Marinelli, E., Grollman, A., & Patel, D. J. (1990) *Biochemistry 29,* 4456–4465]. In our previous paper [Huang, P., & Eisenberg, M. (1992) *Biochemistry 31,* 6518–6532] we established the three-dimensional structure of this X·A 9-mer duplex at pH 5.8 by use of restrained molecular dynamics followed by NOE-based back-calculation refinement. The present paper discusses the structure at pH 8.9 and the pH-dependent conformational transition between the structures at pH 5.8 and at pH 8.9. The structure at pH 8.9 is calculated starting from five different conformations. The final structures converge and agree well with the experimental NOE intensities. These structures are essentially B-type DNA (with X5 and A14 in the B_{II} conformation while the other residues are in the most commonly described B_I conformation) and display an approximate 27° kink at the center of the helix. At the kink site, X5 is positioned in the major groove with the exocyclic ring directed toward the G6·C13 base pair, unstacked from the flanking base G6 and exposed to the solvent. A14, opposite the lesion, remains stacked with its neighbor C15, but not with C13. The kinked helix can accommodate the rotation of the bulky X5 about its glycosidic bond. We propose here a model for the pH-dependent transition. Our model explains the conformational change, which includes the anti and syn rotation of the bulky adduct around its glycosidic bond, with a minimal energy barrier and with an overall kink of the DNA helix. These new findings, fully consistent with the NMR experimental data, were revealed only after restrained dynamics refinement. Distance-restrained energy minimization by itself was insufficient, as shown by the previous NMR study.

Cyclic nucleic acid adducts with mutagenic potential are commonly induced by environmental pollutants. Biological studies (Singer & Bartsch, 1986) have shown that some of these derivatives affect base pairing and induce mutations in DNA. Three-dimensional structures of these adducts in solution are necessary to understand, at the molecular level, how local helix distortions at sites of exocyclic adduct formation may exert effects on DNA replication and repair and lead ultimately to mutagenesis and carcinogenesis.

The 1,N^2-propanodeoxyguanosine adduct (Chart I) is a stable analogue of the adduct generated with acrolein, but lacking the hydroxyl group. Like the naturally occurring mutagenic adduct, upon DNA replication, deoxyadenosine is incorporated preferentially opposite it. It has been shown that this adduct is an excellent model for the acrolein-modified deoxyguanosine (Grollman, 1989). NMR studies (Kouchakdjian et al., 1989, 1990) have demonstrated that the structure of the X·A 9-mer duplex (Chart II) in solution is pH dependent. At pH 5.8 it adopts a conformation which is distinctly different from that at pH 8.9. These two conformations are at equilibrium and are reversible upon pH variation, with different pairing orientations at the lesion site. At pH 5.8, A14 is protonated and X5 adopts a syn orientation. The two hydrogen bonds formed in the protonated X5·A14 pair (Chart III)

Chart I

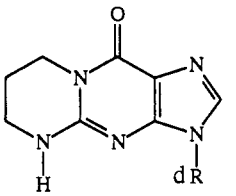

Chart II

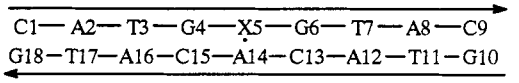

stabilize the low-pH conformation (Kouchakdjian et al., 1989). At pH 8.9, A14 is not protonated and X5 adopts the anti orientation. The pH-dependent conformational equilibrium between the low- and high-pH structures was titrated using NMR measurements, and the pK_a was determined to be 7.6. The exchange between the high- and low-pH conformations is slow on the NMR time scale since resonances from both states were detected at intermediate pH values (Kouchakdjian et al., 1990).

$$\underset{\text{pH = 5.8}}{\text{X5(syn)·A14}^+\text{(anti)}} \underset{pk_a = 7.6}{\rightleftharpoons} \underset{\text{pH = 8.9}}{\text{X5(anti)·A14(anti)}} \quad (1)$$

In our previous study (Huang & Eisenberg, 1992) we determined the low-pH conformation using restrained mo-

† This work was supported by NIH Grants CA47995 and ES0406804 to M.E. and CA49982 to D.J.P.

‡ State University of New York at Stony Brook.

§ Columbia University.

0006-2960/93/0432-3852$04.00/0

Chart III

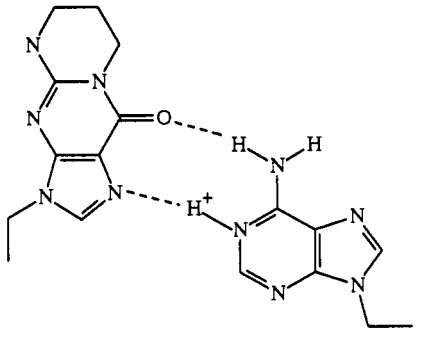

X (syn) A (anti)

lecular dynamics calculations with interproton distances derived from two-dimensional NOE experimental data. Separate simulations started from classical A- and B-form DNA and converged to essentially identical structures. These structures were further refined by a NOE-based back-calculation dynamics simulation which directly minimized the difference between the observed 2D NOE intensities and those calculated from the structures by the full relaxation matrix approach. The final structures obtained were B-type DNA and agreed very well with experimentally observed NOE intensities ("crystallographic" R values of 0.17). These results indicated that the calculations had sampled sufficient conformational space and the converged refined structures represented a reasonable approximation of the actual solution structure at pH 5.8.

In this paper we calculate the structure at high pH via analogous methodology. Even though fully validated simulation protocols for nucleic acids have not yet been unequivocally established, our previous studies (Huang & Eisenberg, 1992) based on NOE experimental data as well as those of others (Nilges et al., 1991; Baleja et al., 1990) suggest that it is reasonable to use distance restraints derived from isolated two-spin approximation for the initial calculations, provided that these are followed by a back-calculation refinement which takes spin diffusion into account. In fact, several studies (Keepers & James, 1984; Borgias & James, 1988; Borgias et al., 1989; Landy & Nagaswara, 1989; Madrid et al., 1989) have shown that neglecting spin diffusion effects can lead to an inaccurate set of distances. Therefore, we chose to use relatively large upper and lower bounds for distances in restrained molecular dynamics simulations and then conducted the back-calculation refinement procedure (Nilges et al., 1991), which incorporates the difference between observed and calculated NOE intensities as an effective energy term and minimizes its derivatives with respect to atomic coordinates (Yip & Case, 1989). The back-calculations, thus, lead to a direct fit to the experimental NOE cross-peak volumes.

The nature of the conformational interchange between the high-pH structure, in which X5 is in the anti orientation, and the low-pH structure, in which X5 is in the syn orientation, is interesting not only from the structural perspective since the rotation of the bulky adduct about its glycosidic bond is expected to be blocked by the stacked flanking base pairs but also from the mutagenic potential at physiological pH where both forms exist at equilibrium. To our knowledge, there have been no reported investigations of this kind of transition in the literature. In this paper, we propose a model that explains the transition of the X·A 9-mer conformations, during which the bulky modified guanine base changes its orientation (anti ↔ syn) depending on the pH in solution and the concomitant protonation of A14.

MATERIALS AND METHODS

(*a*) *Starting Structures.* Since the low-pH structure of the X·A 9-mer duplex had been determined to be B-type DNA, we chose classical B-form DNA as starting structures for calculations at high pH. Five different pairing alignments of X5 and A14 were used to construct the five starting structures. The primary criterion for the selection of our starting structures was that they should sample as much of the conformational space consistent with the experimental data as possible.

The initial model building was carried out on a Evans & Sutherland PS390 graphics workstation driven by an Alliant FX-1 minisupercomputer using the program BioGraf (BioDesign, Inc.). The starting structures were constructed from the classical B-DNA (Arnott & Hukins, 1973) 9-mer with modifications at the lesion site to accommodate five different alignments of X5 and A14, where X5 was derived from the deoxyguanosine base at position 5 incorporating the propano exocyclic bridge. The resultant starting structures are labeled Ini-1 through Ini-5. Stereoviews of the different pairing alignments of X5 and A14 in these starting structures are shown in Figure 1.

(*b*) *Interproton Distances and 2D NOE Volumes.* All NMR experimental data are from the NMR studies (Kouchakdjian et al., 1990) of the X·A 9-mer at pH 8.9, in which two-dimensional phase-sensitive proton NOESY spectra of the X·A 9-mer in D_2O buffer were recorded at mixing times of 50 and 300 ms and the exchangeable proton spectrum in H_2O was recorded at a mixing time of 120 ms. The interproton distances were estimated (Kouchakdjian et al., 1990) from the cross-peak intensities in the NOESY spectra, with broad lower ($\Delta_- = 0.4 \sim 1.2$ Å in D_2O, $\Delta_- = 1.0 \sim 2.0$ Å in H_2O) and upper ($\Delta_+ = 0.7 \sim 1.2$ Å in D_2O, $\Delta_+ = 1.0 \sim 1.2$ Å in H_2O) bounds. A total of 153 experimentally determined distances (87 interresidue and 66 intraresidue) were included in our restrained molecular dynamics simulations.

We measured the volume integrals from the NOESY contour plots using the program Felix (Hare Research, Inc.) on a Silicon Graphics IRIS 4D/220 GTX workstation. The parameters reported in the previous NMR study (Kouchakdjian et al., 1990) were used in our data processing and Fourier transforms with Felix. To measure the volumes, peaks were first located and identified by boxing, and the intensities of the chosen peaks were then quantified by adding up the signal inside the boxes. In some regions of the spectra, however, peaks overlapped significantly. It was not possible to extract accurate intensities from these regions by boxing individual peaks. For this reason, the intensity of a region which contains significantly overlapping peaks was quantified as a single peak, and the NOE restraint was defined for the sum of the proton pairs involved. During NOE-based refinement calculations, the sum of these peaks was compared to the observed volume of the region. A total of 134 (50 ms) and 196 (300 ms) observed volume integrals were collected, and they were used in our NOE-based back-calculation refinements, with a range of ±5% for bounds. The complete tables of volume integrals, interproton distances, and bounds are included in the supplementary material.

(*c*) *Calculations and Analyses.* Computations of energy minimizations, molecular dynamics, and back-calculations were performed with the program X-PLOR (developed by Professor Axel T. Brünger, Yale University). Analyses of structural helical parameters were performed with the program

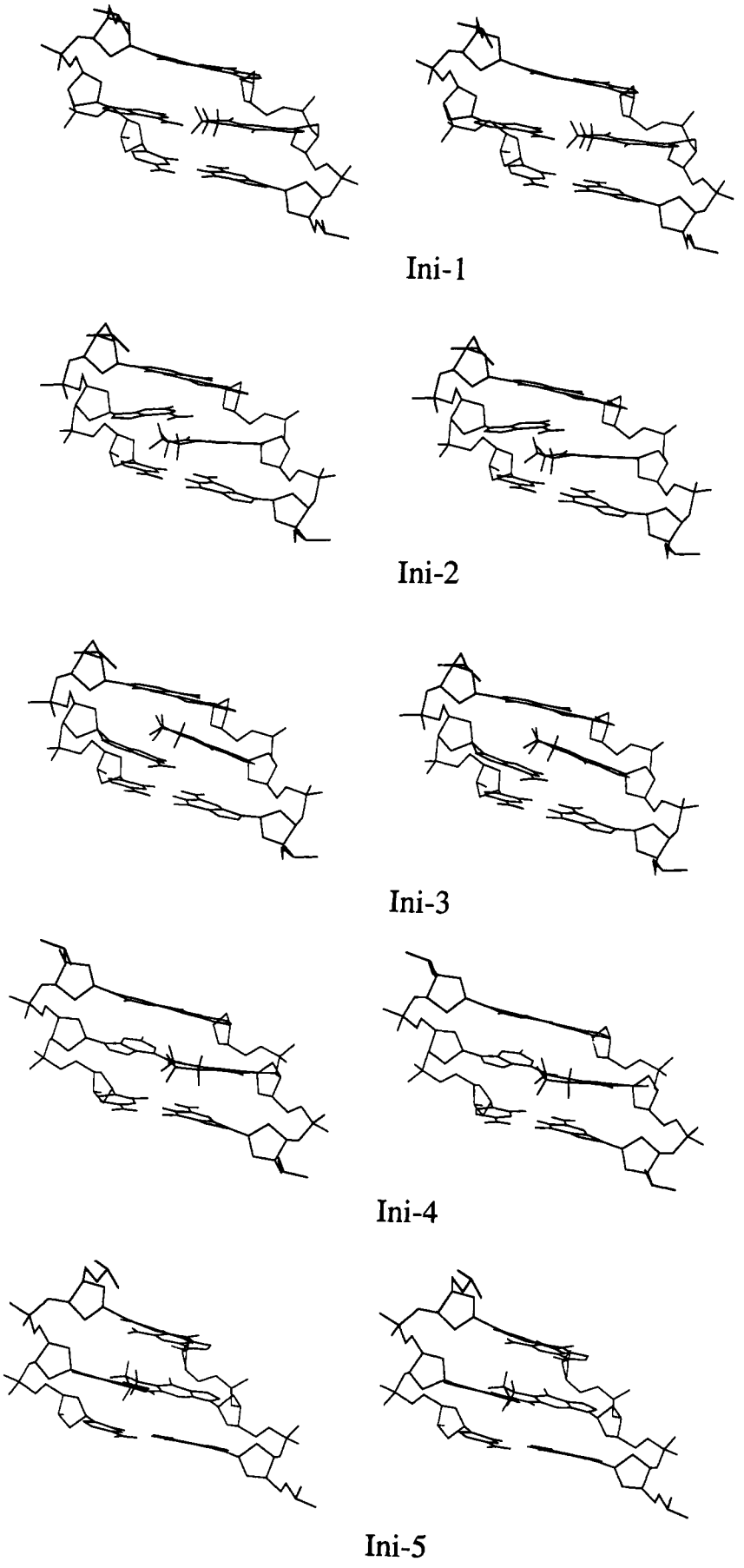

FIGURE 1: Stereoviews of the different pairing alignments of X5 and A14 in the five starting structures (Ini-1, Ini-2, ..., Ini-5). Only the three central base pairs in the structures are displayed.

Dials-and-Windows (provided by Professor G. Ravishanker, Wesleyan University). Molecular graphics displays of structures were produced by the program Midas (obtained from Professor Robert Langridge at the Computer Graphics Laboratory, UCSF). All calculations and displays were executed on a Silicon Graphics IRIS 4D/220 GTX workstation.

The empirical energy function used was that developed by Nilsson and Karplus (1986) for nucleic acids. It consists of the energy terms for bonds, bond angles, dihedral torsions, planar geometries, explicit hydrogen bonding, and nonbonded interactions (van der Waals and electrostatic). The electrostatic potential energy term uses Coulomb's law and is based on a fully charged set of partial charges (−1/residue) with a dielectric constant of 80. The NOE and distance restraining functions used were standard square well effective potentials. Bond lengths involving hydrogen atoms were kept fixed with the SHAKE algorithm (Ryckaert et al., 1977) throughout our calculations. Solvent water molecules and counterions were not included explicitly in our calculations, but their effects may be implicitly reflected by the NOE restraints which are a direct measure of the actual solution structure under the experimental conditions employed.

The three different NOE R values that we used to measure the fit of a refined structure to the NOE data are the "X-ray" R value (analogous to the crystallographic residual index), the "weighted" R value (used in X-PLOR), and the $R^{1/6}$ value (James, 1991). In reality, these R values are calculated following the definitions by Nilges et al. (1991) and can be summarized by a generalized equation:

$$R^n = \sum_{\text{spectra}} \sum_{i=1}^{N_s} [w_i \times well(I_i^c, k_s I_i^o, \Delta_i, n)] / \sum_{\text{spectra}} \sum_{i=1}^{N_s} w_i (k_s I_i^o)^n \quad (2)$$

where I_i^c and I_i^o are the calculated and observed NOE intensities, respectively, Δ_i is the error estimate for I_i^o, w_i is a weight factor, k_s is the calibration factor for each spectrum, and N_s is the number of cross-peaks in each spectrum. The value of the calibration factor k_s is evaluated as

$$k_s = \sum I_i^c / \sum I_i^o \quad (3)$$

The function $well(a,b,\Delta,n)$ is defined as the absolute value of the difference between the nth powers of a and b, where b has an error estimate Δ:

$$\begin{aligned} well(a,b,\Delta,n) &= (b-\Delta)^n - a^n && \text{if } a^n \le (b-\Delta)^n \\ &= 0 && \text{if } (b-\Delta)^n < a^n < (b+\Delta)^n \\ &= a^n - (b+\Delta)^n && \text{if } a^n \ge (b+\Delta)^n \end{aligned} \quad (4)$$

For $n = 1$, $\Delta_i = 0$, and $w_i = 1$, R^n corresponds to the X-ray R value commonly used in crystallography (note that no error offset is used). For $n = 1$, with Δ_i and w_i applied, R^n represents the weighted R value which is closely related to the NOE energy term used by X-PLOR for back-calculations. For $n = {}^1/_6$ R^n corresponds to the $R^{1/6}$ value (James, 1991). No error offset is used for the $R^{1/6}$ value, which is unweighted.

(*d*) *Refinement Protocol.* We used restraints on (a) Watson–Crick base pairing for A·T and C·G base pairs, (b) major groove distances, (c) backbone torsions, and (d) base-pair planes. Lists of these restraints are included in the supplementary material.

In the simulations, each of the initial structures (Ini-1, Ini-2, ..., Ini-5) was subjected to the following refinement protocol with appropriate weights of restraints which are described as k_{dist}(exp) for experimental NOE distances, k_{dist}(hbond) for Watson–Crick base pairings, k_{dist}(grv) for major groove distances, k_{dihe}(backbone) for backbone torsions, k_{dihe}(plane) for base-pair planes, and k_{relax} for NOE volumes.

The starting structures were first subjected to 500 steps of energy minimization, with weight scales of k_{dist}(exp,hbond,grv) = 0.5, k_{dihe}(backbone) = 50, and k_{dihe}(plane) = 30. Then, in each restrained molecular dynamics simulation, two steps at different temperatures were applied: (1) For 7-ps high-temperature (450 K) dynamics, k_{dist}(exp,hbond,grv) was increased from 0.5 to 500 in the first 1 ps by multiplying its value by 2 every 0.1 ps and then remained at 500 throughout the simulation. The initial velocities were assigned with a Maxwell distribution at 450 K. The temperature of the system was maintained at 450 K by rescaling the velocities of atoms every 0.2 ps. The time step of the integrator was set to 0.001 ps. (2) For 15-ps equilibrium (300 K), k_{dist}(exp,hbond,grv) was maintained at 500. The velocities of atoms were rescaled every 0.1 ps to keep the temperature 300 K. The time step of the integrator was 0.001 ps. The coordinates of the last 5 ps were averaged and subjected to restrained energy minimization to generate the restrained dynamics structures, designated as MD-1, MD-2, ..., and MD-5 for those starting from Ini-1, Ini-2, ..., and Ini-5, respectively.

In the back-calculation refinement, structures MD-1, MD-2, ..., and MD-5 were subjected to the following steps, with a uniform isotropic correlation time of 5.0 ns and weight scales of k_{dist}(hbond,grv) = 400, k_{dihe}(backbone) = 30, and k_{dihe}(plane) = 30 no backbone torsion restraints on the three central base pairs and no base-pair plane restraints on the X5·A14 pair). (1) For 25-step energy minimization, k_{dist}(exp) for distances in H_2O is set at 400, k_{dist}(exp) for distances in D_2O at 200 (here, only those distances which involve either X5 or A14 were used), and k_{relax} at 100. (2) For contiguous dynamics stages with time step = 0.5 fs, tolerance = 0.02 Å, and cutoff = 4.5 Å, (a) at 0.5-ps dynamics (300 K), k_{dist}(exp in H_2O) = 400, k_{dist}(exp in D_2O) = 200, and k_{relax} = 100, (b) at 0.5-ps dynamics (300 K), k_{dist}(exp in H_2O) = 400, k_{dist}(exp in D_2O) = 200, k_{relax} = 200, and (c) at 1.0-ps dynamics (300 K), k_{dist}(exp in H_2O) = 400, k_{dist}(exp in D_2O) = 0, and k_{relax} = 400. The final structures R-1, R-2, ..., and R-5, refined from MD-1, MD-2, ..., and MD-5, respectively, were obtained by averaging the coordinate trajectories over the last 0.5 ps followed by 50 steps of energy minimization with only the NOE volume restraints (k_{relax} = 400) and Watson–Crick base-pairing restraints [k_{dist}(hbond) = 400].

During the back-calculation refinements, "tolerance" denotes the maximum distance a hydrogen is allowed to move before the relaxation matrix and gradients are recalculated, and "cutoff" is the radius of the spheres around spins i and j such that only those spins within these spheres contribute to the cross relaxation between spins i and j. The calibration factors k_s were recalculated after the initial minimization and at the end of each dynamics stage in the back-calculation refinement. We chose the isotropic correlation time of 5 ns for all our back-calculations. This correlation time was derived from a comparison of the weighted R values calculated by X-PLOR for the MD structures subjected to refinements over a range of correlation times (1–10 ns). This comparison shows that the R values remained virtually unchanged in the range of correlation times of 4–10 ns but were larger for correlation times of 1–3 ns (data not shown). Coincidentally, the selected correlation time (5 ns) is actually the same as that used in back-calculations for the low-pH conformation (Huang & Eisenberg, 1992).

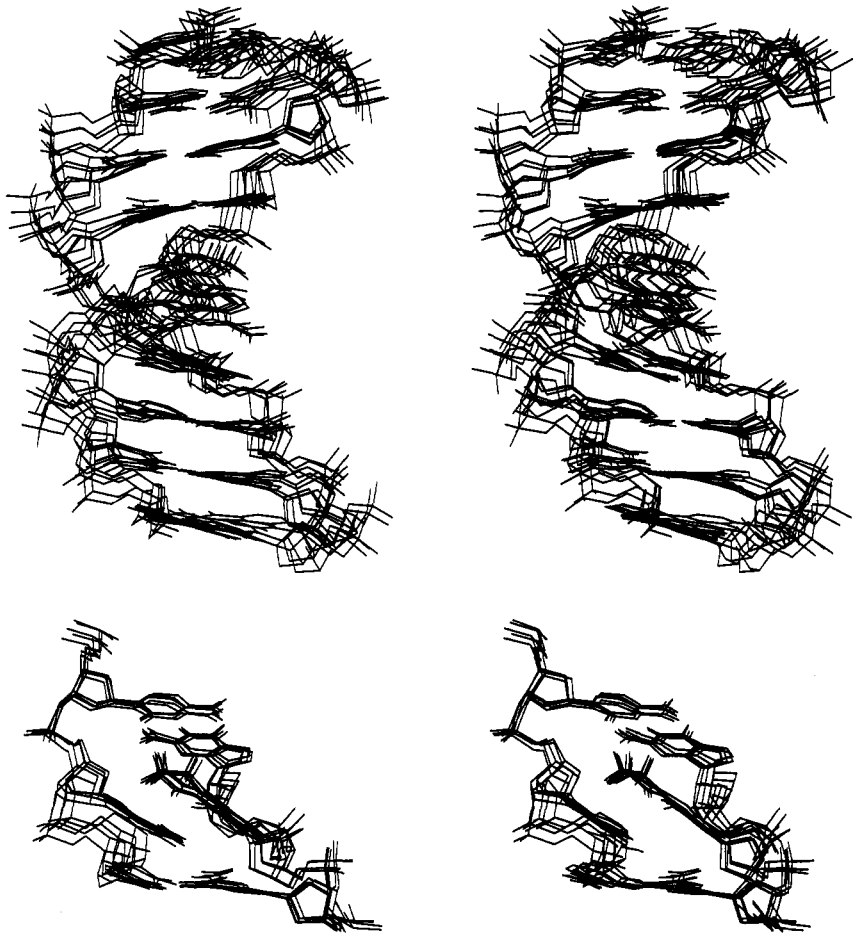

FIGURE 2: (Top) Stereoviews of the superimposed MD structures (MD-1, MD-2, ..., MD-5). (Bottom) Expanded stereoviews of the three central base pairs. They have been rotated by 90° to provide a view of the pairing alignments.

RESULTS AND DISCUSSION

(1) The High-pH Structure

Refined Structures and Their Agreement with Experimental NMR Data. The superimposed distance-restrained molecular dynamics structures (MD-1, MD-2, ..., Md-5) are displayed in Figure 2 (top), and the superimposed final refined structures (R-1, R-2, ..., R-5) are shown in Figure 3 (top). In these figures, the expanded stereoviews of the three central base pairs have been rotated by 90° and displayed at the bottom of each figure for a clearer view of the lesion site. An rms comparison of the final refined structures and the changes in coordinates of the structures at various refinement stages are listed in Table I. The rms comparisons of the final structures show that R-1, R-2, R-3, and R-4 converge to essentially identical structures (rms differences ≤ 1.0 Å). The average of these convergent structures, therefore, has been calculated and shown in Figure 4 (top). For the purpose of comparing high- and low-pH structures, the averaged low-pH structure obtained by us previously (Huang & Eisenberg, 1992) is also displayed in Figure 4 (bottom). The structure R-5 is somewhat different from the convergent set. However, at the lesion site the pairing alignments of X5 and A14 in all final structures are very similar, as shown in Figure 3 (bottom), even though separate simulations started from quite different pairing alignments (Figure 1). These results indicate that the resulting structures do not depend on starting conformations and the simulations performed have overcome energy barriers and sampled sufficient conformational space. The alignments obtained for X5 and A14 are consistent with those proposed by NMR experimental studies (Kouchakdjian et al., 1990). The structural shifts induced by back-calculation refinements are shown by the rmsd of final vs MD structures in Table I, varying from 1.4 to 1.5 Å. This suggests that changes made by back-calculations are similar in all five structures and are simply a consequence of the approximate nature of the distance data used in restrained molecular dynamics. Table I also shows the structural differences between the final and starting structures and between the MD and starting structures.

The agreement of MD structures to experimental interproton distances is shown in Table II. It is clear tht all MD structures satisfy the experimental distance restraints very well, with the rms deviations from experimental distances of only 0.002–0.003 Å and the individual differences ≤ 0.013 Å. These values lend strong support to the veracity of the MD structures. For the back-calculation refined structures (R-1, R-2, ..., R-5), we have measured their deviations from idealized geometry (Table III) and their fit to observed NOE intensities via R values (Table IV). The small values in Table III indicate that the empirical energies have maintained good covalent geometry of structures during the restraining simulations so that no significant distortion in the covalent structures has taken place. In fact, calculations that include the NMR restraints are expected to generate structures that give the best possible fits to NMR data and, at the same time, are the best possible ones energetically with good covalent geometry and nonbonded contacts.

The NOE R values listed in Table IV show the improvement in fit to experimental NOE intensities by simulations. At

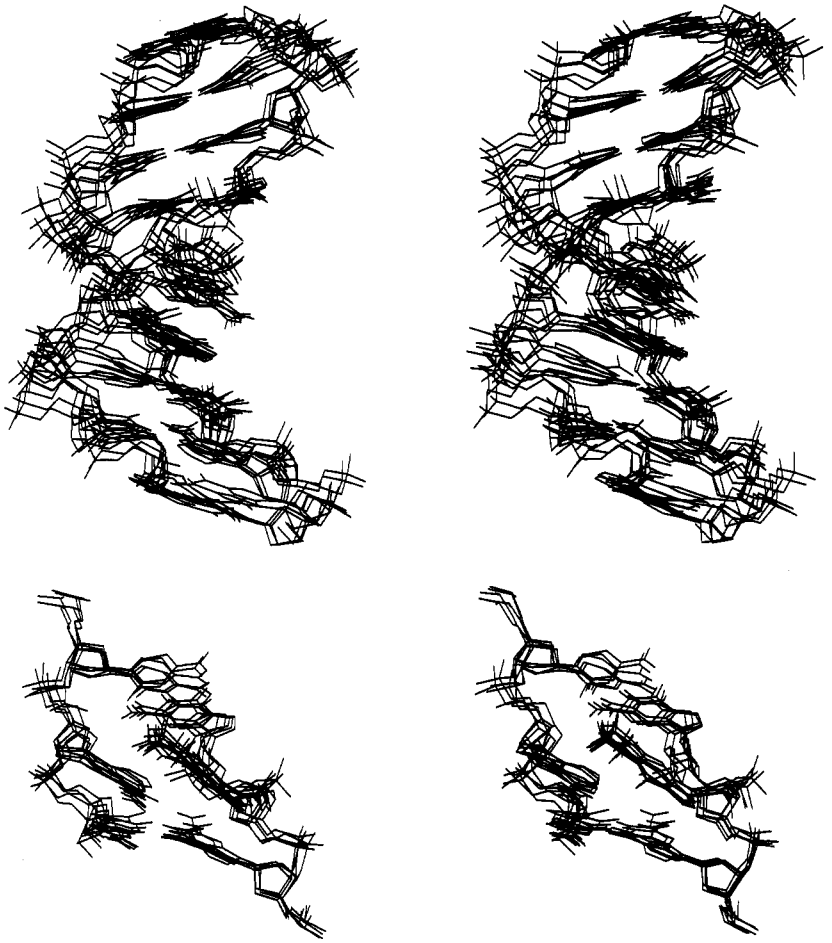

FIGURE 3: (Top) Stereoviews of the superimposed final refined structures (R-1, R-2, ..., R-5). (Bottom) Expanded stereoviews of the three central base pairs. They have been rotated by 90° to provide a view of the pairing alignments.

Table I: rmsd of Structures (pH 8.9)

	rmsd (Å) between the Final Structures			
structure	R-2	R-3	R-4	R-5
R-1	1.04	0.92	0.78	0.70
R-2		0.60	0.80	1.53
R-3			0.76	1.46
R-4				1.20

	rmsd (Å) of Final Structures vs MD Structures				
structures	R-1 vs MD-1	R-2 vs MD-2	R-3 vs MD-3	R-4 vs MD-4	R-5 vs MD-5
	1.41	1.42	1.49	1.43	1.39

	rmsd (Å) of Final Structures vs Starting Structures				
structures	R-1 vs Ini-1	R-2 vs Ini-2	R-3 vs Ini-3	R-4 vs Ini-4	R-5 vs Ini-5
	2.02	2.28	2.09	2.16	2.16

	rmsd (Å) of MD Structures vs Starting Structures				
structures	MD-1 vs Ini-1	MD-2 vs Ini-2	MD-3 vs Ini-3	MD-4 vs Ini-4	MD-5 vs Ini-5
	1.58	1.73	1.68	1.85	1.74

high pH, as compared to our previous low-pH calculations (Huang & Eisenberg, 1992), *R* values are relatively larger. This can be explained as follows. In the low-pH structure, the modified base X5 adopts a syn glycosidic torsion angle, resulting in the bulky propano bridge being directed into the major groove. Few NOEs were observed between the CH_2 in the propano ring and the other bases (only NOEs between CH_2 protons and the H8 proton of the flanking G4 were detected). Thus, the NOESY spectra in D_2O were simpler and well resolved. In the high-pH structure both X5 and A14 are directed toward the interior of the helix, and more NOEs were detected. This resulted in a few crowded and partially overlapped cross-peak regions. The intensities of individual peaks from these regions, therefore, are less precise than those of the low-pH structure. In fact, the *R* values which reflect the fit of the refined structures to NOE data depend not only on the calculated structures but also on the quality of the measured volume data. Therefore, it is not surprising that the *R* values in the refined high-pH structure are relatively larger than those in the refined low-pH structure. However, considering that no error offsets were used in the calculation of our *R* values and that all observed NOE cross-peaks, including those less well defined, were included in the calculation of the *R* values, the calculated high-pH structures satisfy the experimental NOE restraints rather well and are commensurate to those of Nilges et al. (1991).

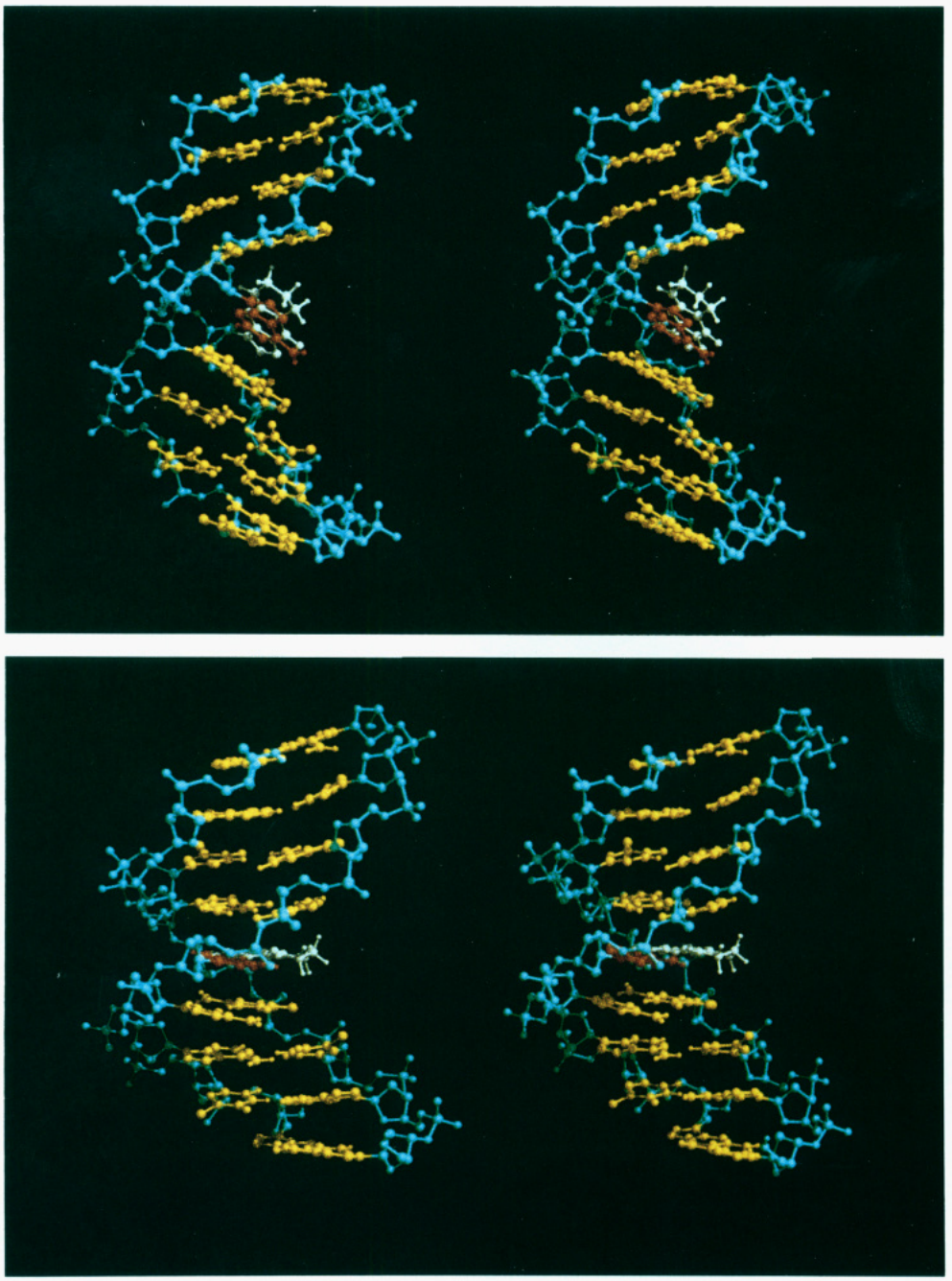

FIGURE 4: Color stereoviews of the high-pH structure (top) and the low-pH structure (bottom) in stick-and-ball model. The modified guanine is white and the adenine, opposite the lesion, is red. The high-pH structure is the average of structures R-1, R-2, R-3, and R-4. The low-pH structure is the average of the structures at pH 5.8 obtained by us previously (Huang & Eisenberg, 1992).

Table II: Agreement of MD Structures to Experimental Interproton Distances

structure	rmsd (Å)	max $\lvert d_{cal} - d_{exp} \rvert$ (Å)
MD-1	0.002	0.013
MD-2	0.002	0.013
MD-3	0.002	0.012
MD-4	0.003	0.013
MD-5	0.002	0.012

Table III: Deviations of the Final Refined Structures from Idealized Geometry

structure	bonds (Å)	angles (deg)	dihedrals (deg)
R-1	0.008	3.978	27.751
R-2	0.008	3.945	28.002
R-3	0.008	3.942	27.860
R-4	0.008	3.956	27.749
R-5	0.008	3.997	27.693

A comparison of the changes in R values during simulations (Table IV) indicates that the significant reduction of R values is a consequence of back-calculations. Distance-restrained molecular dynamics also reduces R values, but not as efficiently. However, from Table I we can see that structural shifts resulting from molecular dynamics (1.58–1.85 Å) are larger than those from back-calculations (1.40∼1.49 Å). In fact, the pairing alignments of X5 and A14 were well established by distance-restrained molecular dynamics and remained essentially unchanged in back-calculations. This can be seen by comparing the pairing alignments of X5 and A14 shown in Figure 2 (bottom) to those in Figure 3 (bottom). Thus, the effect of distance-restrained MD simulations is quite significant, and its role in structural determination of the high-pH conformation cannot be ignored. Although, in principle, one might want to use back-calculations of NOEs directly in

Table IV: NOE R values[a] of the Structures

structure	X-ray	weighted	$R^{1/6}$
Ini-1	0.46	0.62	0.103
Ini-2	0.54	0.86	0.111
Ini-3	0.53	0.80	0.110
Ini-4	0.48	0.90	0.115
Ini-5	0.48	0.84	0.112
MD-1	0.47	0.56	0.094
MD-2	0.48	0.56	0.094
MD-3	0.47	0.55	0.094
MD-4	0.47	0.55	0.094
MD-5	0.48	0.56	0.095
R-1	0.29	0.34	0.069
R-2	0.29	0.34	0.070
R-3	0.29	0.35	0.071
R-4	0.29	0.34	0.070
R-5	0.29	0.34	0.068

[a] These R values follow the definitions in eqs 2–4.

Table V: Comparison of the Experimentally Estimated Distances near the Lesion Site and Those in the Four Convergent Final Refined Structures

proton pair	exptl (Å)	calcd (Å)	
X5(H111/H112)[a]–A14(H2)	3.0–5.2	3.43–4.81	
X5(H101,H102,H121,H122)–A14(H2)	3.3–5.5	3.13–5.24	
X5(H111/H112)–C(13(H1′)	3.3–5.5	4.06–5.24	
X5(H121,H122)–C13(H1′)	2.6–5.6	4.09–4.59	
X5(H111/H112)–A14(H1′)	3.4–5.6	4.76–5.09	[X5(H112)–A14(H1′)]
X5(H111/H112)–A14(H8)	3.0–5.6	4.31–4.49	[X5(H112)–A14(H8)]
C13(H1′)–A14(H8)	2.7–4.4	3.92–5.04	
A14(H1′)–C15(H6)	2.7–4.4	2.88–3.05	
X5(H2′)–G6(H8)	[b]	5.63–5.78	
C13(H2′)–A14(H8)	3.3–5.4	5.40–5.74	
A14(H2′)–C15(H6)	[b]	5.08–5.11	
A14(H8)–C15(H6)	[c]	5.46–5.93	
G4(H3′)–X5(H8)	3.4–5.6	4.81–5.00	
C13(H3′)–A14(H8)	3.4–5.6	4.99–5.58	
A14(H3′)–C15(H6)	3.4–5.6	5.16–5.72	
A14(H8)–A14(H1′)	2.7–4.5	3.95–3.97	
A14(H8)–A14(H2′)	2.2–3.8	2.78–2.81	
A14(H8)–A14(H2″)	2.2–3.4	3.47–3.67	
G6(H1)–X5(H111/H112)	[d]	3.26–4.09	[G6(H1)–X5(H111)]
G4(H1)–A14(H2)	[e]	2.72–3.18	
G6(H1)–A14(H2)	[f]	5.45–6.03	

[a] H111 and H112 are identical in chemical shifts. [b] Very weak or absent. [c] Overlap. [d] Observed in exchangeable proton spectrum (H_2O). [e] Strong in exchangeable proton spectrum (H_2O). [f] Absent in exchangeable proton spectrum (H_2O).

a long molecular dynamics run, thereby eliminating the step of making rather approximate distance determinations, the computational time required would make it impractical at this stage. The major drawback of using the relaxation matrix method in NMR refinement is the high computational cost, since the diagonalization necessary to calculate intensities from each conformation is time consuming (Nilges et al., 1991). Moreover, it is unclear whether structures determined by back-calculating NOEs directly in long molecular dynamics simulations would necessarily be more accurate than those produced by first using approximate distances, followed by refinement with NOEs (Baleja et al., 1990).

To further evaluate the agreement of the calculated structures to the NMR data, a comparison of the experimentally estimated distances near the lesion site and those in the four convergent final refined structures is shown in Table V. It is very clear that our calculated structures are fully consistent with the estimation from NMR data.

To analyze the helical parameters and, consequently, the structural features of the refined structures, we used the program Dials-and-Windows (Ravishanker et al., 1989). The results are shown in Figure 5–7. In these figures, each of the conformational parameters is presented in the form of a dial and each of the helicoidal parameters is drawn on a window. These dials and windows can be compared directly with those for the canonical A-form DNA (Arnott & Hukins, 1972) and B-form DNA (Arnott & Hukins, 1973), shown at the bottom of each figure. Conventions adopted for the presentation of the dials and windows are fully described by Ravishanker et al. (1989). To compare a set of structures, the value of the first structure is drawn as a solid line and the value of every subsequent structure is shown using dashed lines, where the number of dashes is proportional to the index of the analyzed structure (R-2, R-3, R-4, and R-5).

Figure 5 shows the conformational dials for the analyses of torsion angles in the final structures. The 360° conformation wheels ("dials") for each of the backbone dihedral angles, α, β, γ, δ, ϵ, and ζ, the glycosidic bond sugar–base torsion χ, and the sugar pucker ϕ, are presented with reference to successive residues from the 5′ (top) to the 3′ end (bottom). The termini of the chain may have incomplete sets of dials, depending on which atoms are present. The vertical position, corresponding to "north" on a compass wheel, is taken as 0° in the figure. It is clear from the figure that all sugars are puckered in C_2'-endo (refer to the ϕ values) and all bases are in the anti orientation (refer to the χ values). Convergence of the conformational features in the refined structures is observed in the figure: except that A14 in structure R-2 has different α, β, and ϵ values, excellent agreement of torsion angles for the five final structures exists. All residues, excluding X5 and A14, have the backbone torsion angles lying essentially in the conformational range expected for canonical B-form DNA. The backbone conformations of X5 and A14 have changed from the more common B_I conformation ($\epsilon = t$ and $\zeta = g^-$) present in the rest of the structures to the B_{II} conformation ($\epsilon = g^-$ and $\zeta = t$). From these results, the high-pH structures reside clearly in the B-form DNA family. The B_I to B_{II} transitions at X5 and A14 have induced small displacements of the X5 and A14 bases toward the major groove, which can be seen in Figure 3. This positioning implies a special structural feature at the lesion site, where the local backbone distortion from B_I to B_{II} is involved. The occurrence of B_{II} backbone conformation in DNA solution structures, such as the case here, has been reported for an aminofluorene–deoxyguanosine opposite deoxyadenosine containing a DNA 11-mer duplex (Norman et al., 1989) and in adjacent G·A mismatched base pairs in a DNA undecamer (Chou et al., 1992). It was predicted (Norman et al., 1989) that the B_I and B_{II} conformations could be readily interconvertible by changes in environmental conditions. In fact, these two B–form DNA conformations have been observed (Dickerson, 1987; Dickerson et al., 1987) to coexist in a number of crystal structures, with the crystal data suggesting that the energy barrier between the two conformers is modest and surmountable by forces whose magnitudes are comparable to crystal packing forces (Dickerson et al., 1987).

The intra- and inter-base-pair parameters of the helicoidal set are depicted in Figures 6 and 7, respectively, where the parameters referenced to successive base pairs are laid out in the graphics as "windows", defined on a suitable range of values for each parameter. Precise definitions for these parameters are given by Ravishanker et al. (1989). The intra-base-pair parameters, which describe the relative position of bases in a base pair, are shear (SHR), stretch (STR), stagger (STG), buckle (BKL), propeller twist (PRP), and opening

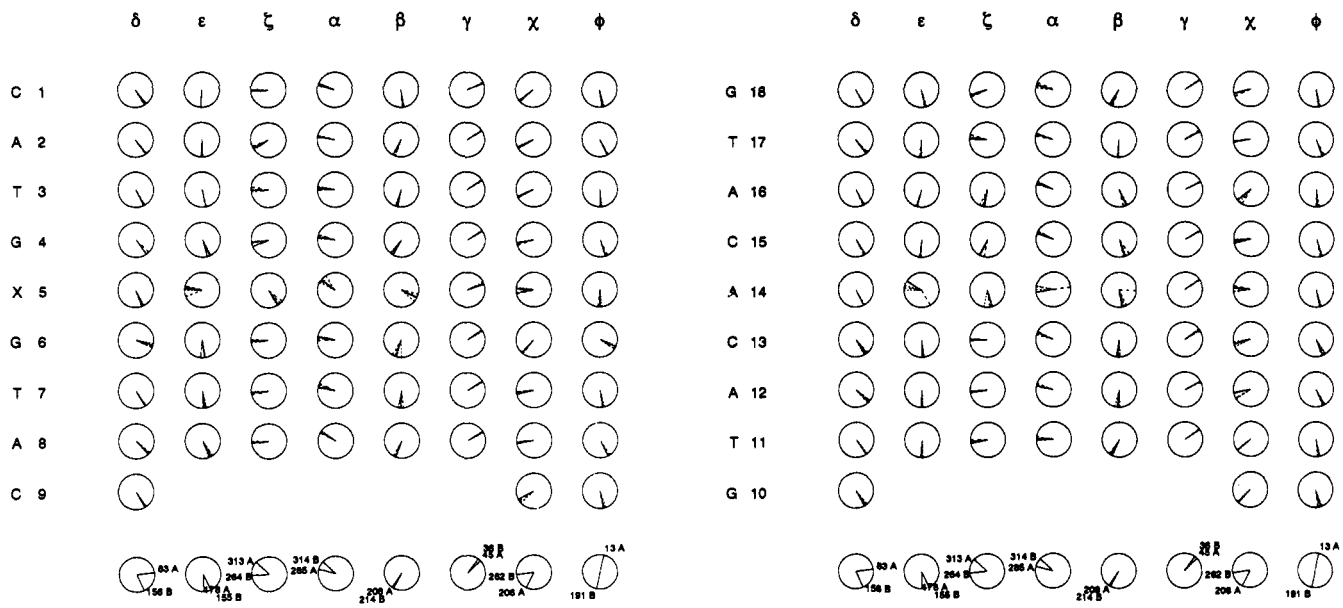

FIGURE 5: Conformational dials for the final refined structures R-1, R-2, ..., and R-5. The value for R-1 is drawn as a solid line, and the value of every subsequent structure is shown using dashed lines with the number of dashes proportional to the index of the analyzed structure. The dials for canonical A-form (Arnott & Hukins, 1972 and B-form (Arnott & Hukins, 1973) DNA are shown at the bottom with the actual values.

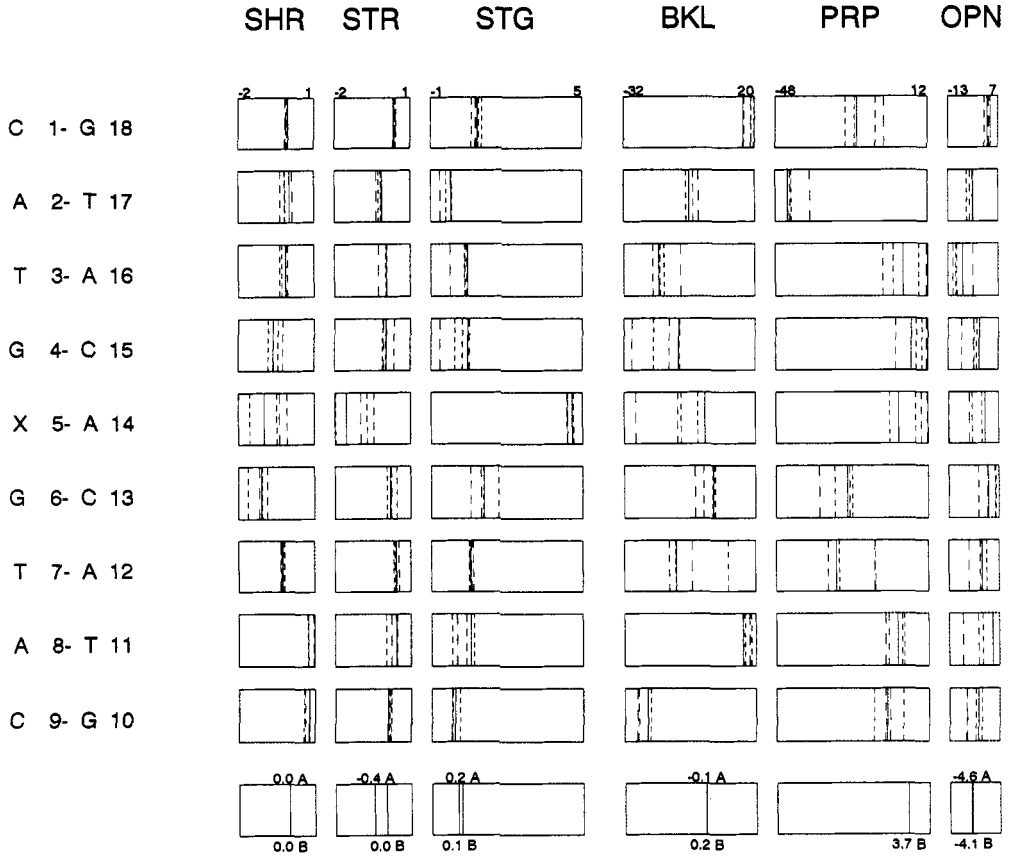

FIGURE 6: Helicoidal windows for intra-base-pair parameters of the final refined structures R-1, R-2, ..., and R-5. The value for R-1 is drawn as a solid line, and the value of every subsequent structure is shown using dashed lines with the number of dashes proportional to the index of the analyzed structure. The windows for canonical A-form (Arnott & Hukins, 1972) and B-form (Arnott & Hukins, 1973) DNA are shown at the bottom with the actual values.

(OPN). Since X5 and A14 are not really on the same plane (see Figure 3), the intra-base-pair parameters are not useful for the X5·A14 pair. Figure 6 shows that the intra-base-pair parameters for the refined structures are similar to the values for canonical A- and B-form DNA (ignore the X5·A14 pair), except that there is some degree of buckling (BKL) in most base pairs and notable propeller twist (PRP) in C1·G18, A2·T17, G6·C13, and T7·A12 pairs. This indicates that Watson–Crick base-pairing character in canonical DNA is retained for all base pairs, with the exception of the X5·A14 pair, in the final structures. The inter-base-pair parameters, which describe the relative position of successive base pairs, are shift (SHF), slide (SLD), rise (RIS), tilt (TLT), roll (ROL), and twist (TWS). As shown in Figure 7, these inter-

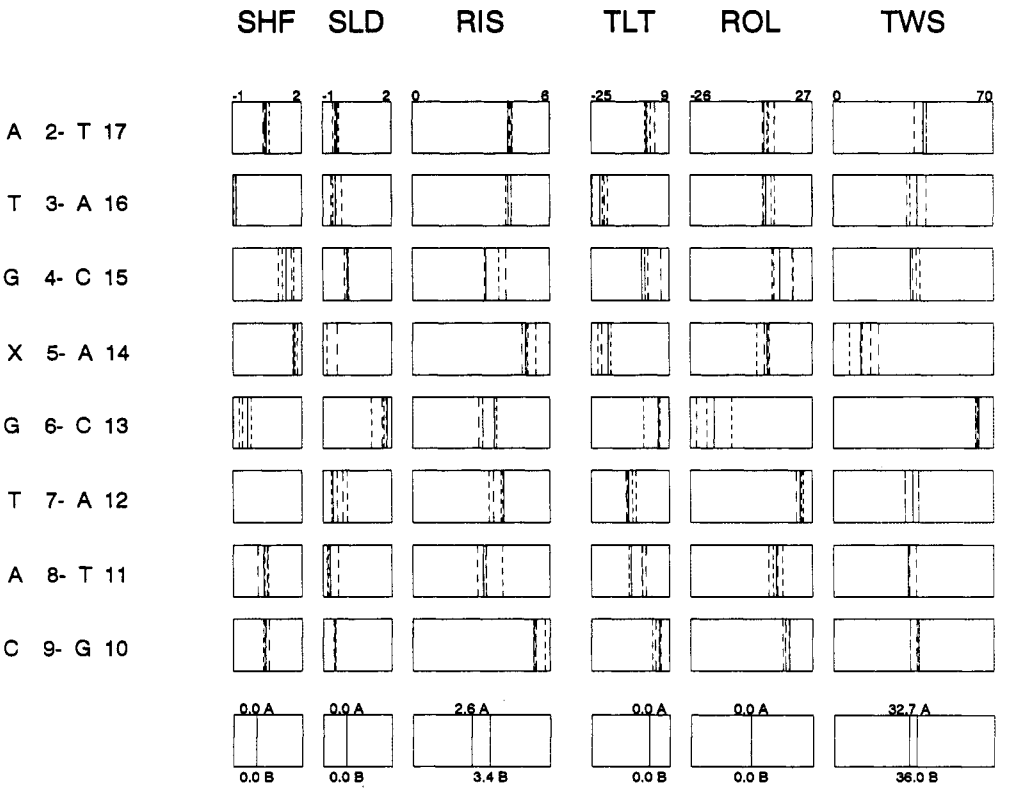

FIGURE 7: Helicoidal windows for inter-base-pair parameters of the final refined structures R-1, R-2, ..., and R-5. The value for R-1 is drawn as a solid line, and the value of every subsequent structure is shown using dashed lines with the number of dashes proportional to the index of the analyzed structure. The windows for canonical A-form (Arnott & Hukins, 1972) and B-form (Arnott & Hukins, 1973) DNA are shown at the bottom with the actual values.

base-pair parameters for most adjacent pairs in the refined structures are close to those for canonical DNA, except for the fourth base-pair step (between base pairs of G4·C15 and X5·A14) and the fifth base-pair step (between base pairs of X5·A14 and G6·C13). Obviously, there is an abrupt structural distortion occurring at the lesion rate. This can be understood by examination of the refined structures in Figure 3 (top) which reveal a kink at the X5·A14 site. From Figure 7, it can be seen that this kink can be attributed to the abnormally low twist angle and the moderately high negative tilt angle in the fourth base-pair step and the high twist value combined with positive slide and large negative roll in the fifth base-pair step. Among these peculiarities, it is noted that the negative roll angle in the fifth base-pair step opens the kink toward the minor groove at the center of the molecule. This results in a marked narrowing of the minor groove at the central base pair. However, this narrowing occurs only locally on the X5·A14 base pair. It does not affect the minor groove at the other base pairs. This can actually be seen in Figure 3 (top). Figure 3 (bottom) shows an expanded view of the portion at the kink site of the molecule. It is clear that X5 in refined structures is positioned in the major groove with the exocyclic ring directed toward the middle of G6·C13 base pair and A14 directed toward the G4·C15 base pair. The helices in these structures are kinked, with X5 completely unstacked from the flanking base G6 (but partially stacked with G4) and exposed to the solvent. A14 remains stacked with C15, but not with C13. In addition, the positioning of A14, relatively close to the adjacent base pair G4·C15, brings into hydrogen-bonding proximity the N6 of A14 and the O6 of G4 (this distance in the averaged high-pH structure is 3.21 Å), thus allowing the formation of a bifurcated hydrogen bond (Taylor et al., 1984).

The Kinked Helix. The most striking feature of the high-pH structures obtained is the kinked helix. Bending is a known conformational change of the DNA double helix. DNA may bend as a result of interaction with proteins or small drugs. DNA can also assume a bent conformation by itself (intrinsic bending). Wu and Crothers (1984) have proposed molecular models for bending which include smooth curvature along the helix and localized bends such as at kinks and junction bends. There is currently much interest in sequence-specific bends in DNA structures (DiGrabriele et al., 1989). These bends appear to occur in AT-rich regions and exhibit smooth curvatures. Abrupt bends or kinks in DNA have been suggested to occur at periodic intervals in chromatin (Crick & Klug, 1975; Sobell et al., 1976). Model studies (Sobell et al., 1976, 1977) have indicated that kinking is made possible by altering the normal C2′-endo deoxyribose sugar ring puckering in B-form DNA to a mixed sugar puckering pattern of the type C3′-endo (3′–5′) C2′-endo and partially unstacking base pairs. A kinking scheme such as this would require minimal stereochemical rearrangement and would also involve small energy barriers. Theoretical calculations (Pack et al., 1977; Vasilescu et al., 1978) have demonstrated that the kinked form becomes a low-energy conformation under conditions in which the phosphate oxygens are neutralized. AT-rich regions should be preferentially kinked under neutralizing conditions. Direct observations of protein-induced DNA kinking in the DNA–cAMP receptor protein complex by electron microscopy (Gronenborn et al., 1984) and in the crystalline DNA–*Eco*RI endonuclease complex by X-ray crystallography (Frederick et al., 1984) support the hypothesis that kinking may indeed be important in DNA–protein interactions. Recent gel electrophoresis studies (Hsieh & Griffith, 1989; Wang & Griffith, 1991) on deletions of bases in one strand of duplex DNA have shown that bulged bases kink duplex DNA, with

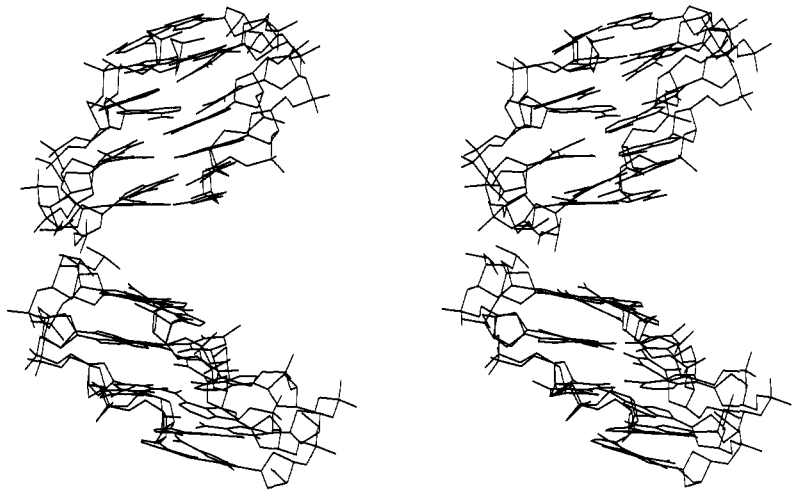

high and low pH structures

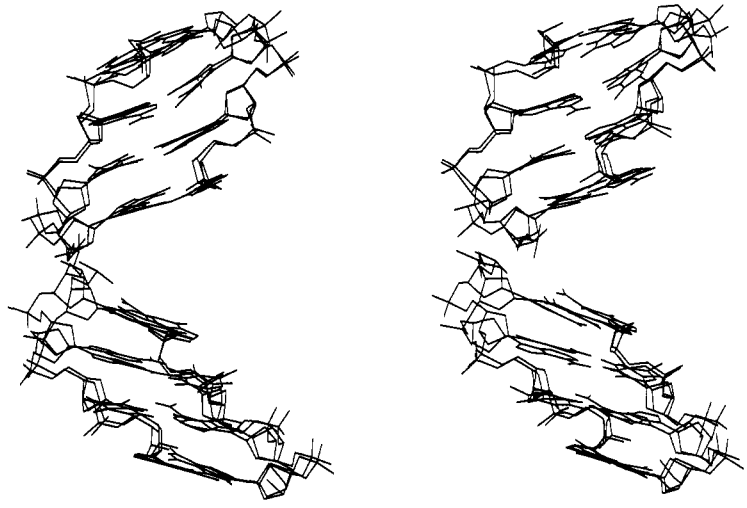

low fit to high pH structure

FIGURE 8: Least-squares fits of segments 1 and 2 in the low-pH structure to those in the high-pH structure. Segment 1 is defined as the four lower base pairs, and segment 2 is defined as the four upper base pairs. The middle X5·A14 base pair is ignored in this figure.

the degree of kinking increasing in roughly equal increments as the number of bases in the bulge increases from one to four. These have been explained in terms of junctions which contain bulged bases between two duplex segments and produce kinks that hold the two duplex segments at precise angles relative to each other.

In our case, as can be seen in Figure 4 (top) which shows the average of the set of convergent refined structures, the helix axis in the X·A 9-mer duplex (pH 8.9) is bent, with the X5·A14 base pair as a pivotal joint about which the kink occurs. This suggests that the kink of the helix is induced by X5 which is not hydrogen bonded to A14 at high pH. Kinks like this may be similar to those (Hsieh & Griffith, 1989; Wang & Griffith, 1991) produced by bulged bases. The possibility that kinks in these cases are induced by unpaired bases in DNA is supported by the fact that analogous kinks have not been observed in the low-pH conformation (Huang & Eisenberg, 1992) of the X·A 9-mer duplex, as shown in Figure 4 (bottom), which has the hydrogen-bonded X5·A14 base pair at the center of the helix.

Examination of the high-pH structure shown in Figure 4 (top) establishes that the kink in the helix is about 27°. This has actually been calculated by separating each of the structures in Figure 4 into two segments so that segment 1 consists of the four lower base pairs and segment 2 consists of the four upper base pairs (the X5·A14 base pair is ignored). This is followed by fitting the coordinate set of each segment in the low-pH structure to the corresponding segment in the high-pH structure. The fittings of segments are carried out by the program X-PLOR and illustrated in Figure 8. Results of the least-squares fits indicate that a rotation of 14° is needed to transform segment 1 and of 13° to transform segment 2. The rms differences between the high- and low-pH coordinate sets are only 0.83 Å in segment 1 and 0.74 Å in segment 2. They are well within the structural rms differences in the set of convergent refined structures (Table I). This suggest that both segments 1 and 2 are essentially unchanged by pH, but only their overall positions are altered. This conclusion is fully consistent with the NMR results that the proton chemical shifts of C1, A2, T3, T7, A8, C9, G10, T11, A12, A16, T17, and G18 in the X·A 9-mer at pH 8.9 are quite similar to those at pH 5.8 [a comparison of the proton chemical shifts at pH 5.8 (Kouchakdjian et al., 1989) with those at pH 8.9 (Kouchakdjian et al., 1990) indicates that the proton chemical shift differences in these residues are mostly $\leq$0.08 ppm but are mostly $\geq$0.2 ppm in and near the lesion site]. These

arguments support the fact that segments 1 and 2 can be assumed to be "rigid" in the transition between high- and low-pH conformations. On the basis of these observations and the established high- and low-pH structures, a model of the transition for the X·A 9-mer conformations as a function of pH is proposed.

(2) Transition between High- and Low-pH Conformations

As shown by Figure 4 (top), the double helix of the high-pH structure exhibits a kink of approximately 27° toward the minor groove. At the kink site, X5 is completely unstacked from the flanking base G6 and is exposed to the solvent. The presence of the kink in the DNA's axis allows X5 to lie in the major groove and thus readily accommodates X5's rotation about its glycosidic bond toward the side of the G6·C13 base pair. This is necessary for the conversion from the high-pH conformation, which has X5 in anti orientation, to the low-pH conformation, which has X5 in syn orientation, by rotating X5 about the glycosidic bond. The rotation of X5 is illustrated in Figure 9. As can be seen, no steric clashes are expected when X5 rotates toward G6·C13, even though X5 is bulky. In contrast, however, if the helix was straight, the bulky X5 would be prevented from rotating by the flanking base pairs.

To study the driving force for X5 to change its orientation when pH in solution is varied, let us focus on the local structure near the lesion site. Figure 10 shows the geometry and van der Waals surfaces of the nucleoside X5 when its base is in syn and in anti orientations. In the anti conformation the six-membered rings of the base are pointing away from the sugar, and therefore, there is no particular steric hindrance between the sugar and base. But, in the syn conformation, the bulky part of the base is located over and toward the sugar, giving rise to close interatomic contacts. It is expected, thus, that X5 prefers the anti orientation.

At pH 5.8 A14 is protonated and there are two interstrand hydrogen bonds which stabilize the low-pH structure, with X5 in syn orientation. This essentially locks the structure in the syn form. But when the pH is raised and A14 loses its protonation, the hydrogen bond involving that proton at A14 is broken. Interstrand hydrogen bonds in the X5·A14 base pair are hence reduced to one, and the unfavorable close interatomic contacts between X5 and A14 become predominant. In this case, the structure is unstable. On the basis of this and the fact that X5 prefers the anti orientation, X5 will tend to change from the syn to the anti conformation to minimize the unfavorable contacts. In addition to this driving force, a strong van der Waals repulsion is expected between the propano bridge of X5 and its flanking base G4 when X5 is in syn orientation, as shown in Figure 11. These forces can all be relieved by kinking the helix and rotating X5 to the anti orientation. This is facilitated, in part, by the B_I in low-pH conformation to B_{II} in high-pH conformation transitions at the X5 and A14 residues, which have induced small displacements of X5 and A14 toward the major groove. The kinked helix can accommodate the rottion of X5 about the glycosidic bond, and thus X5 turns around and goes to the anti orientation. The energy barrier for kinking the helix in this case is expected to be low since there is no hydrogen-bonded base pair in the middle of the helix. This assumption can actually be supported by the fact that existence of kinks has been demonstrated experimentally in doubel-helical DNA which contains extra unpaired or bulged bases (Hsieh & Griffith, 1989; Wang & Griffith, 1991).

In contrast with the low-pH case, the base of X5 at high pH is in the anti orientation. There is no particular driving force for it to convert to the syn form. However, the kinked helix at high pH allows the base of X5 to rotate relatively freely and adopt the syn orientation temporarily. If the pH is low enough for A14 to become protonated, then two interstrand hydrogen bonds between X5 and A14 are formed (Chart III) and X5 will stay in the syn orientation. This is concomitant with the unkinking of the helix such that X5 and A14 can stack with their flanking bases, and the structure is thus further stabilized. This change is facilitated, in part, by the B_{II} to B_I conformational transitions at the X5 and A14 residues. At this point, the high-pH conformation is completely converted to the low-pH conformation.

Proposed Model of the Transition and Kinking Scheme. To describe the interchange betwen low- and high-pH structures, we propose a model of the transition as follows. Low- to high-pH conformation: As the pH in solution is raised, the helix kinks while the hydrogen bonding formed by protonation of A14 breaks. This kink is a consequence of the unfavorable van der Waals contacts in the syn conformer and is accommodated by the B_I to B_{II} conformational transitions at X5 and A14. Subsequently, the base X5 rotates from the syn to the anti orientation. The resultant structure is the high-pH conformation. High- to low-pH conformation: X5 has some rotational freedom, and it can reach the syn orientation, even though the anti orientation is preferred. As the pH is decreased, the interstrand hydrogen bond involving protonation of A14 is formed. The helix, then, unkinks while X5 and A14 stack with their flanking bases. This is facilitated by the B_{II} to B_I conformational transitions at X5 and A14. The resultant structure is the low-pH conformation. Since these changes are reversible and pH dependent, a rapid equilibrium between the low- and high-pH structures exists in solution at intermediate pHs.

The sequence we used to obtain the proposed kinking scheme is as follows: The two segments in the low-pH structure (see Figure 8) transform simultaneously following the equation derived by the program X-PLOR:

$$\mathbf{r}' = [R] \times \mathbf{r} + \mathbf{T} \qquad (5)$$

where $\mathbf{r}'$ is the transformed coordinate set and $\mathbf{r}$ is the original coordinate set. [R] is the rotation matrix and $\mathbf{T}$ is the translation vector. The net result of transformation is that segment 1 is rotated 13.9° about the axis (–0.558 0.691 –0.459) and translated by the translation vector $\mathbf{T}$ = (–1.326 –0.864 0.959) while segment 2 is rotated 13.2° about the axis (0.697 –0.694 –0.180) and translated by the translation vector $\mathbf{T}$ = (2.938 3.215 –1.509). To create a hypothetical kinking trajectory, the set of overall operations, i.e., rotations and translations of the segments, could be divided into equivalent sequential sets of suboperations. At each step a set of suboperations were applied to the segments to generate an intermediate. In this way, a kinking scheme of the structure can be made. The scheme proposed requires minimal stereochemical rearrangement and probably involves small energy barriers. Spectroscopic experiments on the same DNA duplex containing propanodeoxyguanosine opposite adenine show that the free energy difference between the low- and high-pH structures is minimal (Plum, 1992).

The discussion of the transition between high- and low-pH structures prompted us to ask whether we could start a dynamics simulation from the low-pH conformation to achieve the high-pH conformation. We have hence performed the calculation, but no conformational transition of X5 from syn to anti was observed in a 22-ps simulation. This is probably because the rate of this conversion, which was estimated

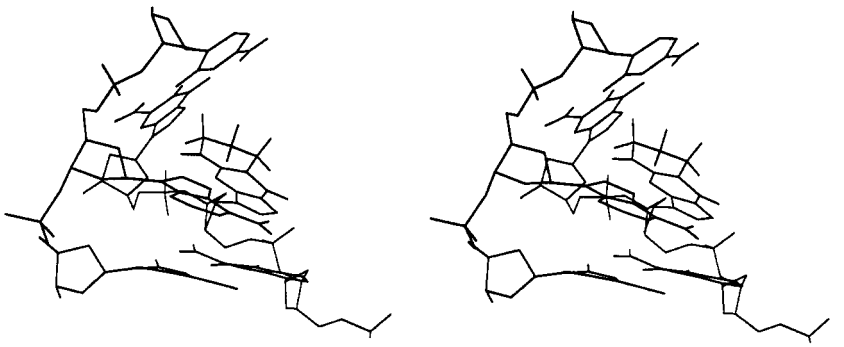

0° rotation

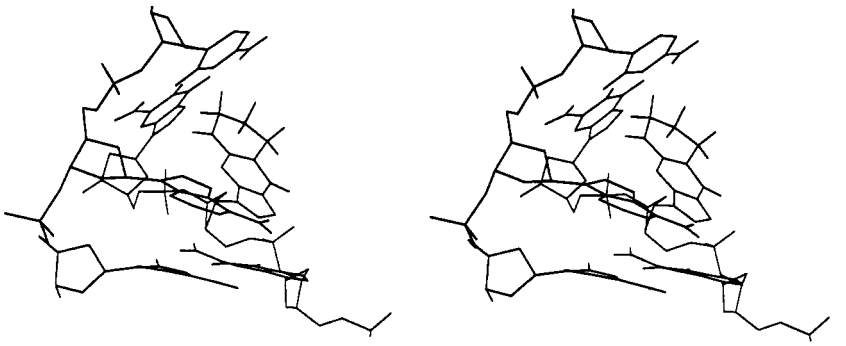

15° rotation

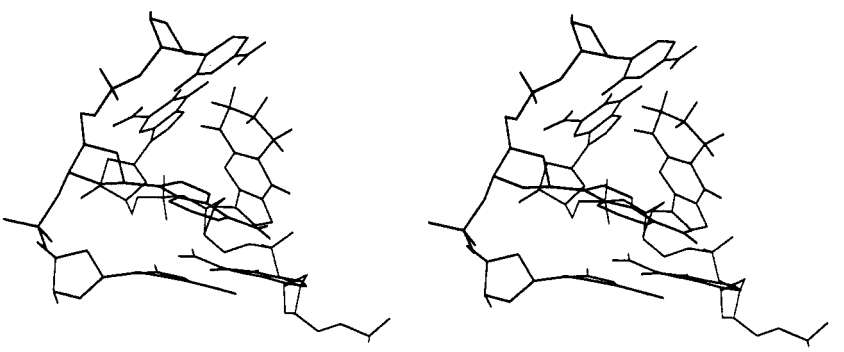

25° rotation

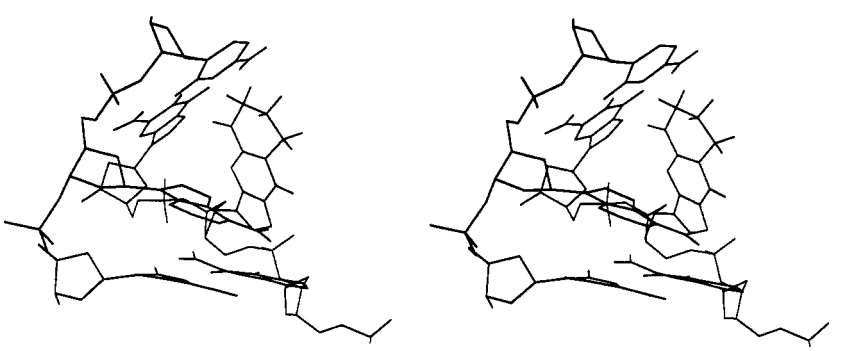

35° rotation

FIGURE 9: Rotation of X5 about its glycosidic bond toward the side of the G6·C13 base pair: (1) 0° rotation; (2) 15° rotation; (3) 25° rotation; (4) 35° rotation.

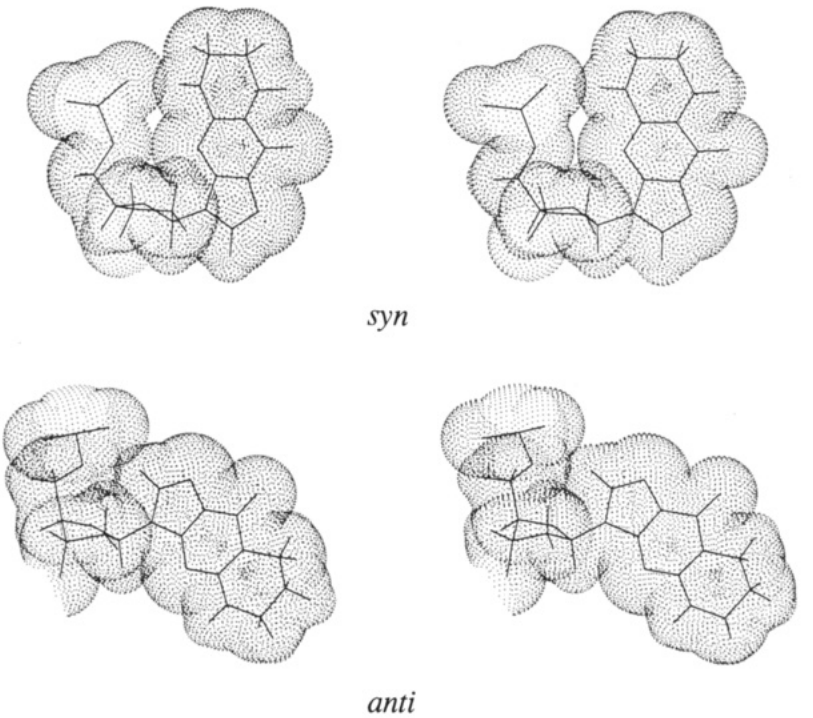

FIGURE 10: Steric hindrance between the base and sugar of X5 when the base is in syn and in anti orientations. The structures are those of the high- and low-pH structures shown in Figure 4.

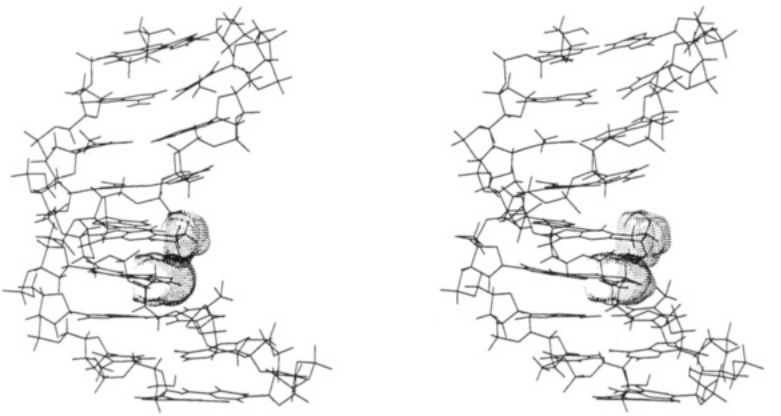

FIGURE 11: van der Waals repulsion between the propano bridge of X5 and its flanking base G4 and X5 is in syn orientation.

(Kouchakdjian et al., 1990) to be less than 900 s^{-1}, would require a much longer MD simulation to observe the transition. Although at this point in time we cannot trace the precise trajectory of conformational transition of the 9-mer duplex in solution, our proposed model of the transition and the kinking scheme are fully consistent with the structural analyses of the established high- and low-pH structures.

CONCLUSIONS

The present study has established the three-dimensional structure of the X·A 9-mer duplex in solution at pH 8.9 by use of distance-restrained molecular dynamics followed by NOE-based back-calculation refinements. The structures obtained display an approximate 27° kink of the helix at the lesion site, where X5 is positioned in the major groove with the exocyclic ring directed toward the G6·C13 base pair, completely unstacked from the flanking base G6 and exposed to the solvent. A14 remains stacked with C15, but not with C13. The alignment of X5 and A14 differs from that in the low-pH conformation. This reflects the interplay between steric and hydrogen-bonding contributions to the stabilization of the modified site.

We have discussed the nature of the pH-dependent conformational change of the X·A 9-mer in solution and proposed a model which provides insights into the transition. Biological studies (Grollman, 1989) on this exocyclic adduct have demonstrated that it has mutagenic potential at physiological pH and replication is significantly slowed down, with deoxyadenosine incorporated preferentially opposite the lesion. To address the structural basis for this, our current hypothesis is that, at the replication fork, 1,N^2-propanodeoxyguanosine exists in both syn and anti conformations. The anti conformation prevents the replication and is consistent with the slowing down of the replication. The syn conformation allows the incorporation of deoxyadenosine opposite it by forming two interstrand hydrogen bonds. Once the duplex is formed, the high- and low-pH structures are at equilibrium. On the second round of replication, the deoxyadenosine will code for a thymine and lead to the G → T transversion.

ACKNOWLEDGMENT

We thank Professor Axel T. Brünger for the X-PLOR program and Dr. M. Nilges for helpful discussions and

Professor G. Ravishanker for the helix analysis program Dials-and-Windows.

SUPPLEMENTARY MATERIAL AVAILABLE

Three tables showing volume integrals for the X·A 9-mer (pH 8.9) at mixing times of 50 and 300 ms and interproton distances with lower and upper bounds and a list of restraints on Watson–Crick base pairing, on major groove distances, on backbone torsions, and on base-pair planes (11 pages). Ordering information is given on any current masthead page.

REFERENCES

Arnott, S., & Hukins, D. W. (1972) *Biochem. Biophys. Res. Commun. 47*, 1504–1509.

Arnott, S., & Hukins, D. W. (1973) *J. Mol. Biol. 81*, 93–105.

Baleja, J. D., Moult, J., & Sykes, B. D. (1990) *J. Magn. Reson. 87*, 375–384.

Borgias, B. A., & James, T. L. (1988) *J. Magn. Reson. 79*, 493–512.

Borgias, B. A., Koning, T. M. G., Van Der Marel, G. A., Van Boom, J. H., & Kaptein, R. (1989) *J. Magn. Reson. 82*, 290–308.

Chou, S., Cheng, J., Fedoroff, O. Y., Chuprina, V. P., & Rein, B. R. (1992) *J. Am. Chem. Soc. 114*, 3114–3115.

Crick, F. H. C., & Klug, A. (1975) *Nature 255*, 530–533.

Dickerson, R. E. (1987) *Unusual DNA Structures* (Wells, R., & Harvey, S., Eds.) Springer-Verlag, New York.

Dickerson, R. E., Goodsell, D. S., Kopka, M. L., & Pjura, P. E. (1987) *J. Biomol. Struct. Dyn. 5*, 557–580.

DiGrabriele, A. D., Sanderson, M. R., & Steitz, T. A. (1989) *Proc. Natl. Acad. Sci. U.S.A. 86*, 1816–1820.

Frederick, C. A., Grable, J., Melia, M., Samudzi, C., Jen-Jacobsen, L., Wang, B. C., Greene, P., Boyer, H. W., & Rosenberg, J. M. (1984) *Nature 309*, 327–331.

Grollman, A. P. (1989) *Proc. Am. Assoc. Cancer Res. 30*, 682.

Gronenborn, A. M., Nermut, M. V., Easton, P., & Clore, G. M. (1984) *J. Mol. Biol. 179*, 751–757.

Hsieh, C. H., & Griffith, J. D. (1989) *Proc. Natl. Acad. Sci. U.S.A. 86*, 4833–4837.

Huang, P., & Eisenberg, M. (1992) *Biochemistry 31*, 6518–6532.

James, T. L. (1991) *Curr. Opin. Struct. Biol. 1*, 1042–1053.

Keepers, J. W., & James, T. L. (1984) *J. Magn. Reson. 57*, 404–426.

Kouchakdjian, M., Marinelli, E., Gao, X., Johnson, F., Grollman, A., & Patel, D. J. (1989) *Biochemistry 28*, 5647–5657.

Kouchakdjian, M., Eisenberg, M., Live, D., Marinelli, E., Grollman, A., & Patel, D. J. (1990) *Biochemistry 29*, 4456–4465.

Landy, S. B., & Nagaswara, R. B. (1989) *J. Magn. Reson. 83*, 29–43.

Madrid, M., Mace, J. E., & Jardetzky, O. J. (1989) *J. Magn. Reson. 83*, 267–278.

Nilges, M., Habazettl, J., Brünger, A. T., & Holak, T. A. (1991) *J. Mol. Biol. 219*, 499–510.

Nilsson, L., & Karplus, M. (1986) *J. Comput. Chem. 7*, 591–616.

Norman, D., Abuaf, P., Hingerty, B. E., Live, D., Grunberger, D., Broyde, S., & Patel, D. J. (1989) *Biochemistry 28*, 7462–7476.

Pack, G. R., Muskavitch, M. A., & Loew, G. (1977) *Biochim. Biophys. Acta 478*, 9–22.

Plum, E. (1992) *Biochemistry* (in press).

Ravishanker, R., Swaminathan, S., Beveridge, R. L., & Sklenar, H. (1989) *J. Biomol. Struct. Dyn. 6*, 669–699.

Ryckaert, J. P., Cicotti, G., & Berendsen, H. J. C. (1977) *J. Comput. Phys. 23*, 327–337.

Singer, B., & Bartsch, H. (1986) *The Role of Cyclic Nucleic Acid Adducts in Carcinogenesis and Mutagenesis*, IARC Scientific Publications 70, International Agency for Research on Cancer, Lyon, France.

Sobell, H. M., Tsai, C., Gilbert, S. G., Jain, S. C., & Sakore, T. D. (1976) *Proc. Natl. Acad. Sci. U.S.A. 73*, 3068–3072.

Sobell, H. M., Tsai, C., Jain, S. C., & Gilbert, S. G. (1977) *J. Mol. Biol. 114*, 333–365.

Taylor, R., Kennard, O., & Versichel, W. (1984) *J. Am. Chem. Soc. 106*, 244–248.

Vasilescu, D., Broch, H., & Cabrol, D. (1978) *Int. J. Quantum Chem., Quantum Biol. Symp. 5*, 345–354.

Wang, Y. H., & Griffith, J. D. (1991) *Biochemistry 30*, 1358–1363.

Wu, H., & Crothers, D. M. (1984) *Nature 308*, 509–513.

Yip, P., & Case, D. A. (1989) *J. Magn. Reson. 83*, 643–648.